



Simulation of river plume behaviors in a tropical region: Case study of the Upper Gulf of Thailand

Xiaojie Yu^a, Xinyu Guo^{a,*}, Akihiko Morimoto^a, Anukul Buranapratheprat^b

^a Center for Marine Environmental Studies (CMES), Ehime University, Japan

^b Department of Aquatic Science, Faculty of Science, Burapha University, Thailand

ARTICLE INFO

Keywords:

River plume
Low latitude
Wind effect
River discharge
Upper Gulf of Thailand
Bulge size

ABSTRACT

River plumes are a general phenomenon in coastal regions. Most previous studies focus on river plumes in middle and high latitudes with few studies examining those in low latitude regions. Here, we apply a numerical model to the Upper Gulf of Thailand (UGoT) to examine a river plume in low latitudes. Consistent with observational data, the modeled plume has seasonal variation dependent on monsoon conditions. During south-westerly monsoons, the plume extends northeastward to the head of the gulf; during northeasterly monsoons, it extends southwestward to the mouth of the gulf. To examine the effects of latitude, wind and river discharge on the river plume, we designed several numerical experiments. Using a middle latitude for the UGoT, the bulge close to the river mouth becomes smaller, the downstream current flows closer to the coast, and the salinity in the northern UGoT becomes lower. The reduction in the size of the bulge is consistent with the relationship between the offshore distance of a bulge and the Coriolis parameter. Momentum balance of the coastal current is maintained by advection, the Coriolis force, pressure gradient and internal stresses in both low and middle latitudes, with the Coriolis force and pressure gradient enlarged in the middle latitude. The larger pressure gradient in the middle latitude is induced by more offshore freshwater flowing with the coastal current, which induces lower salinity. The influence of wind on the river plume not only has the advection effects of changing the surface current direction and increasing the surface current speed, but also decreases the current speed due to enhanced vertical mixing. Changes in river discharge influence stratification in the UGoT but have little effect on the behavior of the river plume.

1. Introduction

In coastal regions, the discharge of freshwater from rivers is one of the principle sources of buoyancy. Through formation of a river plume with a sharp density gradient between the buoyant freshwater and sea water, two notable characteristics emerge in the Northern hemisphere: an anticyclonic bulge in the vicinity of the river mouth and a downstream (in a Kelvin wave sense) coastal current (Chao and Boicourt, 1986). The behavior of the plume is influenced by a variety of factors, including wind (Fong, 1998; Dzwonkowski et al., 2014), the Coriolis force (Kasai et al., 2000; Fong and Geyer, 2002), ambient currents (Fong and Geyer, 2002), tides (Guo and Valle-Levinson, 2007; Horner-Devine et al., 2009), thermal stratification (Wang et al., 2008) and river discharge (Yankovsky et al., 2001; Wang et al., 2011; Dzwonkowski et al., 2014).

Most studies on river plumes are based on observations or model analysis conducted in middle or high latitude regions, such as the Chesapeake Bay (Pritchard, 1952, 1954; Guo and Valle-Levinson,

2007), Delaware Bay (Münchow and Garvine, 1993; Wong, 1994), the Columbia River (Horner-Devine et al., 2009), and the Yellow River (Wang et al., 2008, 2011). However, fewer studies examining river plume behaviors have been conducted in regions of low latitude. Low latitude regions have a small Coriolis parameter, enormous discharges of freshwater and distinctive wind patterns (Nittrouer and DeMaster, 1996). All of these factors make the behavior of river plumes in low latitudes significantly different from those in middle and high latitudes.

The main focus on tropical rivers has been on the Amazon River (Lentz and Limeburner, 1995; Lentz, 1995a, 1995b; Nittrouer and DeMaster, 1996), which discharges freshwater at the equator. Differing from river plumes in middle latitudes, which deflect to the right by the Coriolis force in the Northern Hemisphere, the Amazon River plume extends leftward to the north Brazilian shelf between the equator and 5°N under the superposition effects of the low latitude location, strong tides and easterly trade winds (Lentz, 1995a; Nittrouer and DeMaster, 1996). There are also other rivers in low latitude regions, not just around the equator, but between the equator and middle latitudes.

* Correspondence to: Center for Marine Environmental Studies, Ehime University, 2–5 Bunkyo-cho, Matsuyama 790-8577, Japan.
E-mail address: guoxinyu@sci.ehime-u.ac.jp (X. Guo).

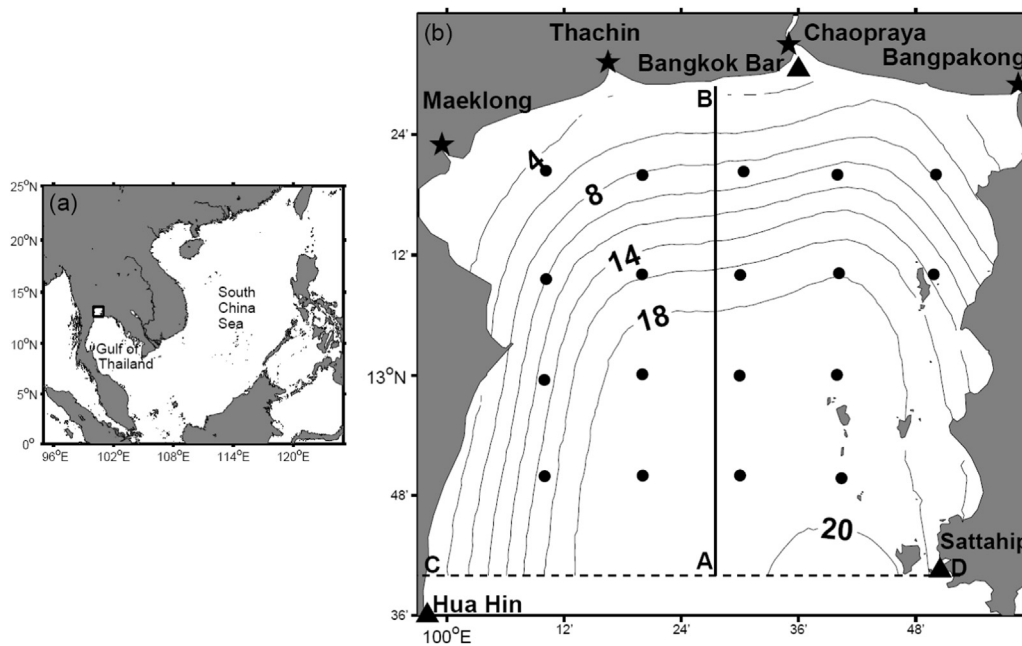


Fig. 1. (a) Location and (b) bathymetry (m) of model domain in the Upper Gulf of Thailand (UGoT). Stars indicate the positions of the river mouths of the Maeklong, Thachin, Chaopraya, and Bangpakong, respectively. Solid circles show the stations where observational data are available for 2014 and 2015. Triangles indicate observation stations for tidal harmonic constants, namely Hua Hin, Sattahip and Bangkok Bar, respectively. Section AB is indicated by the solid line. Line CD shows the position of the open boundary of the model.

They may not be subject to persistent large river inflows and easterly trade winds, but have seasonal variations in river discharge and wind patterns such as those in middle latitude regions. Here, we examine the behavior of a river plume in a tropical region, the Upper Gulf of Thailand (UGoT, Fig. 1), which has seasonal variations in river discharge and is subject to monsoons.

The UGoT, which is a semi-enclosed shallow sea located in a tropical region at about 13°N, has characteristics of estuarine-like systems due to large freshwater discharges. The sea is surrounded by land on the eastern, northern and western sides and is connected to the main Gulf of Thailand at its southern boundary (Fig. 1a). The maximum depth is approximately 20 m in the southeastern part of the UGoT. Four rivers, namely, the Maeklong, Thachin, Chaopraya and Bangpakong from west to east (Fig. 1b), discharge freshwater into the gulf. The seasonal variation in discharges of these rivers is apparent, with smaller discharges from December to May and larger discharges from June to November. The UGoT is also subject to monsoons with dry northeasterly winds from November to January and wet southwesterly winds from May to September.

A study on the seasonal variation of water column conditions in the UGoT (Buranapratheprat et al., 2008) revealed that strong stratification develops in September and October when river discharge is large and heat flux is moderate, while the water column becomes well mixed in December and January due to surface heat loss, lower discharge from rivers and strong inputs of wind stress. Using a three-dimensional model, Buranapratheprat et al. (2009) showed that monsoons determine seasonal circulation in the UGoT, which is clockwise during southwesterly monsoons and counter-clockwise during northeasterly monsoons. However, they did not pay special attention to the dynamics of river plumes in the UGoT. Using a numerical model, Saramul and Ezer (2014) evaluated dynamics in the UGoT, which are influenced by surface heat flux, river runoff, and low latitude. They found that the extension of river plumes differs under different monsoon conditions. The larger Coriolis parameter in middle latitudes in their model likely pushes the plume farther along the west coast and makes the plume near the river mouth less axisymmetric. However, the larger Coriolis parameter cannot lead the plume to turn more to the right, for which they did not give an explanation. Due to insufficient information on the river plume in the UGoT, as well as the potential contribution of river water-induced stratification to the generation of hypoxia (Green et al., 2006), which could have severe consequences on the coastal

ecosystems in the UGoT, it is necessary to enhance our understanding of the distribution of the river plume in the UGoT and its contribution to stratification. In this study, our objective is to investigate the dynamics responsible for the river plume and stratification in the UGoT, including the influences of low latitude, wind and river discharge, through three-dimensional numerical modeling.

In Section 2, we briefly introduce *in situ* data collected in the UGoT and model configuration. After comparison of the model results with observational data, the modeled behaviors of the river plume and the induced stratification in the UGoT under monsoons will be described in Section 3. In Section 4, we examine the influences of low latitude, wind and river discharge on the river plume in the UGoT through a series of numerical experiments. The study is summarized in Section 5.

2. Observational data and model description

Water temperature and salinity data were collected at 0.1 m intervals through the entire depth at 18 stations (black points, Fig. 1b) once in August, September, November and December 2014 and in February, April and June 2015 in the UGoT. Using these observational data, we determined seasonal variations in the horizontal and vertical distributions of water temperature and salinity, thereby identifying the presence of a river plume.

In order to understand the distribution and controlling factors of the observed river plume, we developed a numerical model for the UGoT. The model is based on the Princeton Ocean Model (POM), which is a three-dimensional, primitive equation, sigma-coordinate model (Blumberg and Mellor, 1987; Mellor, 2003). The vertical diffusivity coefficients are calculated by a second momentum turbulent closure scheme (Mellor and Yamada, 1982), and the horizontal diffusivity coefficients are parameterized by the Smagorinsky formulation (Smagorinsky, 1963). The model domain and bathymetry are shown in Fig. 1b. Spatial resolution is ~1 km in the horizontal direction and 21 sigma layers in the vertical direction, with higher resolution in the surface and bottom layers than in the middle layer.

For external forcing, we consider monthly heat flux (Fig. 2a), monthly river discharges (Fig. 2b), and monthly wind stresses (Fig. 2c), all of which represent climatologic conditions and are from Buranapratheprat et al. (2008). The net heat flux is the sum of the sensible heat flux, latent heat flux, long wave radiation and short wave radiation, and has small seasonal variation with a maximum value in

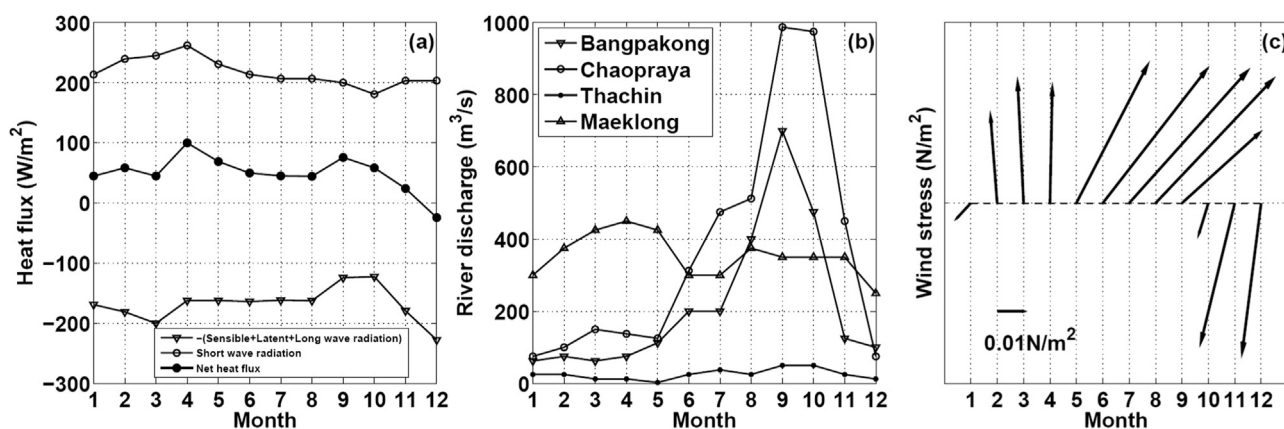


Fig. 2. (a) Monthly heat flux (W/m^2), (b) monthly river discharges (m^3/s), and (c) monthly wind stress (N/m^2) in the UGoT.

April ($\sim 100 W/m^2$) and a minimum value in December ($\sim -30 W/m^2$). Due to the small area of the UGoT (approximately $100 km \times 100 km$), we specified a spatially uniform heat flux in the model.

The model includes the discharges from four rivers, namely the Maeklong, Thachin, Chaopraya and Bangpakong (Fig. 1b), among which the Chaopraya is the largest. Seasonal variations in discharges from the Chaopraya and Bangpakong rivers (Fig. 2b) are the most extreme, with small outputs from December to May ($100 - 200 m^3/s$) but large outputs from August to November ($500 - 1000 m^3/s$). The Maeklong and Thachin rivers have smaller seasonal variation in discharges, and the former has a large discharge ($\sim 300 m^3/s$) while the latter has a small discharge ($< 50 m^3/s$) throughout the year.

Wind in the UGoT shows seasonal variations (Fig. 2c), with southerly to southwesterly winds from February to September, northeasterly winds in November and December, and a transitional period in January and October. We specified a spatially uniform wind stress in the model due to the small area of the UGoT. It should be noted that the period with large river discharges coincides with the three stages of monsoon (September, October and November), which can make the behavior of the river plume variable.

Along the open boundary of the model in the UGoT, monthly water temperature and salinity data from Buranapratheprat et al. (2009) are applied. Four tidal constituents, M_2 , S_2 , K_1 and O_1 with harmonic constants at two stations (Hua Hin and Sattahip) near the open boundary from Buranapratheprat et al. (2009) are added to the elevation at the open boundary.

The model calculation was started from the rest state in January with a total integration period of 3 years. The model results were saved at 1-h intervals. A tide filter (Hanawa and Mitsudera, 1985) was used to remove tidal components. The analysis reported here is based on model results in the third year (case 0), which nearly coincide with those in the second year.

3. Results

3.1. Validation of model results through comparison with observations

Since tidal motion is important for determining the behavior of river plumes (Guo and Valle-Levinson, 2007), four major tidal constituents (M_2 , S_2 , O_1 and K_1) are considered in our model. To assess model performance, we compare the modeled tidal harmonic constants of the four tidal constituents with observations at one station, the Bangkok Bar station (position shown in Fig. 1b). Since the area of the UGoT is small, the comparison with observation data at one station (Bangkok Bar) in the head of the bay enables us to confirm the simulation of tides over entire bay. Comparisons between model results and observations indicate good prediction of tidal constituents in the UGoT by the model (Table 1). The tidal range is about 50 cm from the south to the north of

Table 1

Comparison of harmonic constants of four tidal constituents between observations and model results at one station in the UGoT. The phase is with reference to $105^\circ E$.

Harmonic constituents	Bangkok Bar Amplitude (cm) Phase ($^\circ$)
Observed K_1	67.0 167.0
Modeled K_1	66.6 167.7
Observed O_1	46.0 117.1
Modeled O_1	45.3 122.5
Observed M_2	55.0 141.0
Modeled M_2	51.5 146.7
Observed S_2	27.0 212.0
Modeled S_2	27.0 223.6

the UGoT.

Water temperature and salinity in the UGoT show strong seasonal variations (Figs. 3 and 4). We selected February and September to represent different monsoonal seasons, respectively, because both heat flux and river discharge have different patterns in these two months. In February, the observed water temperature is about $27.5 - 27.7^\circ C$ over the entire UGoT (Fig. 3a), and the water column is vertically homogeneous (Fig. 3e) due to surface heat loss and strong winds. In September, the temperature is higher than $30^\circ C$ and shows a little spatial variation, with the northeast of the UGoT around $1.0^\circ C$ lower than the southwest (Fig. 3c). Meanwhile, stratification develops in the water column (Fig. 3g). In the northeast of the UGoT, water temperature at the surface ($29.6^\circ C$) is slightly lower than that at the bottom ($30.1^\circ C$). Temperature inversion is not unusual in coastal regions affected by large river discharge in a cooling season (Thadathil et al., 2002). In the latter part of September, surface temperature in the UGoT begins to decrease due to surface heat loss. At the same time, river discharge increases substantially. Consequently, the low salinity water at the surface keeps the low temperature surface water lighter than the high temperature bottom water.

The modeled water temperature is generally consistent with observational data if we consider that the observations were in 2014 and 2015, while the model is based on climatologic conditions. The modeled water temperature in February (Fig. 3b, f) is slightly warmer ($\sim 0.1^\circ C$) than the observation, but is also vertically homogeneous. In September, the modeled temperature (Fig. 3d, h) is slightly lower ($\sim 0.3^\circ C$) than the observation, but the pattern of a lower temperature in the northeast than the southwest is consistent with the observation. Moreover, a higher temperature at the bottom than at the surface is also reproduced by the model (Fig. 3h).

Being similar to water temperature, the observed salinity is also vertically homogeneous in February and has slight spatial variation with a lower value in the west (32.0) than in the east (32.2) (Fig. 4a, e), which is likely induced by the relatively large river discharge from the

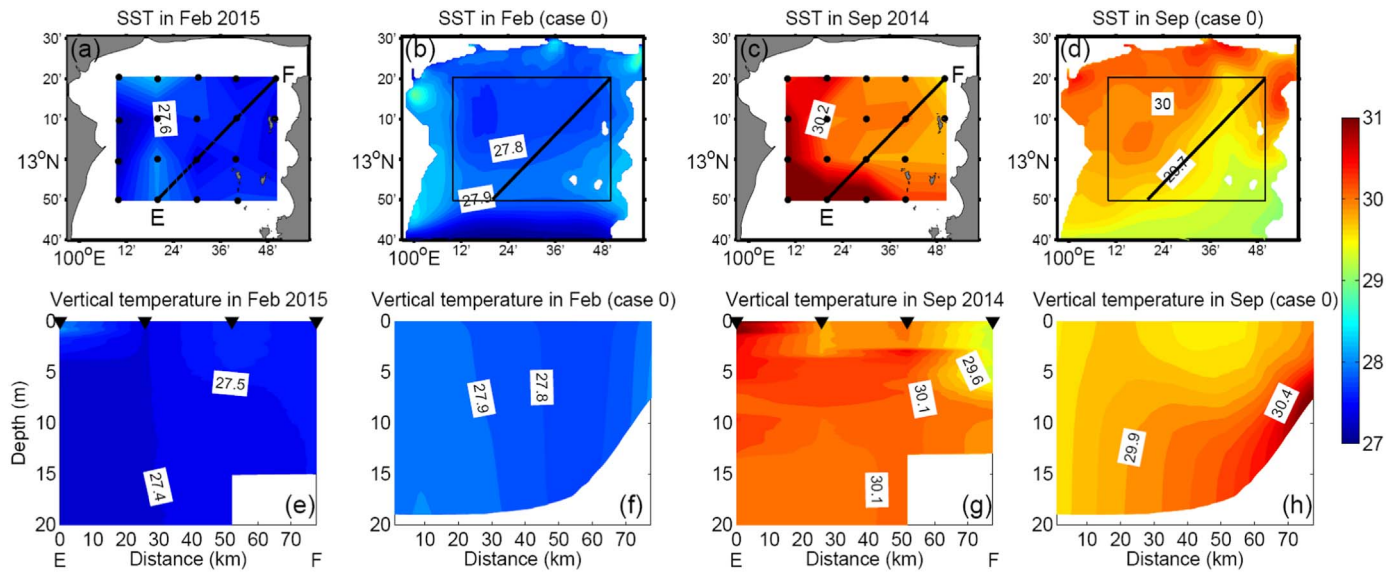


Fig. 3. Horizontal (top) and vertical (bottom) distributions of observational data (a, c, e, g) and model results (b, d, f, h) for water temperature (°C) in February and September in the UGoT. The vertical distribution is shown in section EF in (a) to (d).

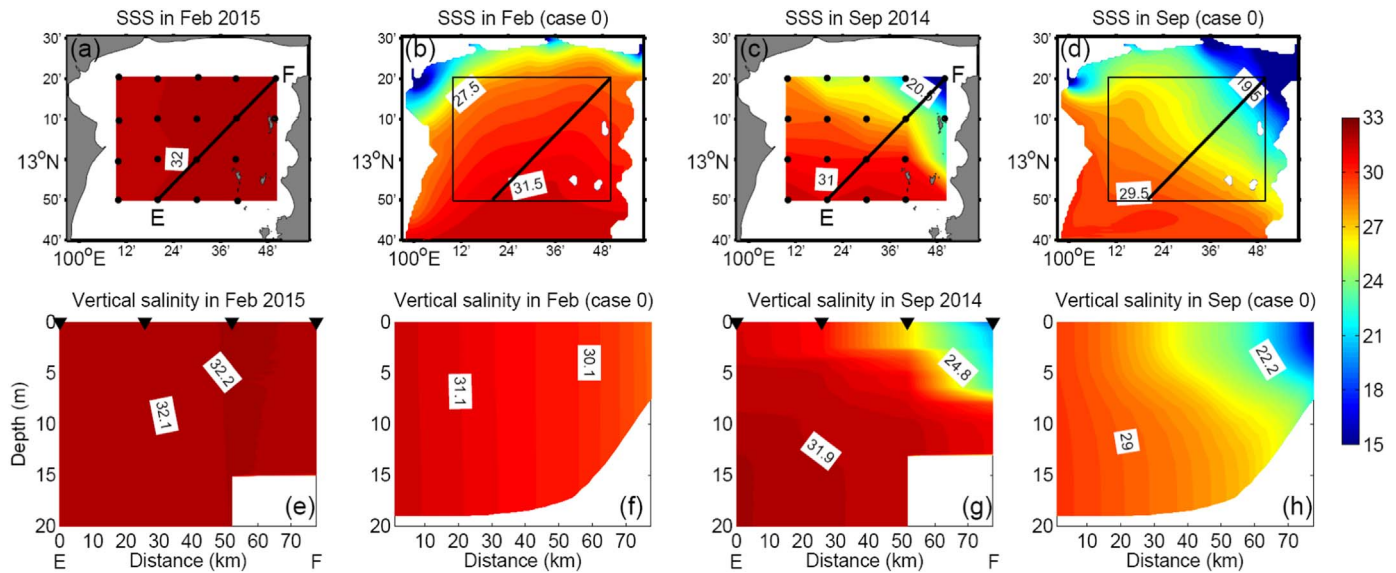


Fig. 4. The same as Fig. 3 but for salinity.

Maeklong. In September, salinity decreases greatly and shows apparent spatial variation with low salinity (< 20) in the northeast and high salinity (~31) in the southwest (Fig. 4c). Meanwhile, strong stratification occurs in the northeast with low salinity water above high salinity water (Fig. 4g). The salinity given by the model generally reflects the pattern of the observation. In February, the modeled salinity is smaller in the northwest than in the southeast (Fig. 4b), and is also vertically homogeneous (Fig. 4f). In September, the salinity decreases greatly, and has large spatial variation with lower salinity (< 20) in the northeast and higher salinity (~29.5) in the southwest (Fig. 4d), and is strongly stratified in the northeast (Fig. 4h). The spatial and vertical patterns are consistent with the observations, although the modeled salinity values are lower than the observations. This discrepancy is mainly caused by the external forcing used in the model for river discharge and wind, which are climatological conditions instead of actual observed conditions. However, this discrepancy has little influence on the behaviors of the plume noted by this study.

3.2. River plume affected by monsoons in the UGoT

To examine the effect of monsoons on the behavior of the river plume, we compared model results for salinity and residual currents in September, October and November, when monsoons are forced by the southwesterly wind, weak transitional wind and northeasterly wind, respectively.

In September (Fig. 5a), the prevailing southwesterly wind drives the low salinity water from the largest river, the Chaopraya, to the eastern UGoT, and therefore hinders the westward extension of the plume. Freshwater from the Bangpakong remains near the river mouth, which results in a large salinity gradient around the river mouth. The plume of the Maeklong extends upstream to the northeast under the influence of the southwesterly wind. The spatial distribution of salinity shows a pattern of gradually increasing from the northeast to the southwest of the UGoT. The residual current with an average velocity of about 0.08 m/s flows southeastward under the southwesterly wind.

In October (Fig. 5b), when the northeasterly wind is relatively weak and river discharge is still large, low salinity water from the Chaopraya

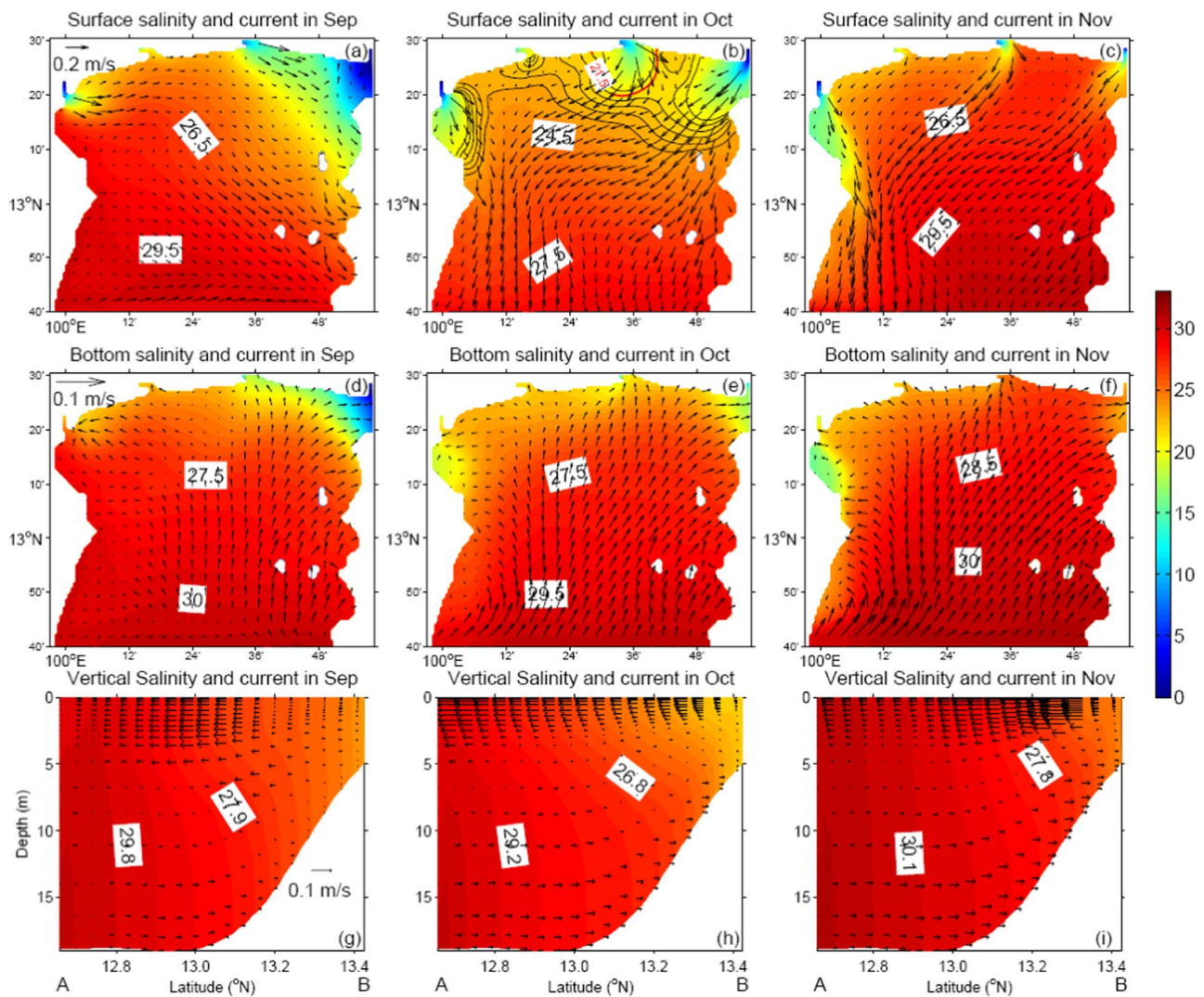


Fig. 5. Horizontal distribution of modeled salinity (color) and residual current (m/s, arrows) in the surface layer (top) and bottom layer (middle), and vertical distribution of salinity (color) and current along section AB (m/s, arrows) (bottom) in September, October and November for case 0. The position of section AB is shown in Fig. 1b. The black lines in (b) show the isohalines around the bulge, and the red line indicates the position of the offshore distance of the bulge. Note that the scales for current speed are different for these distributions. (For interpretation of the references to color in this figure legend, the reader is referred to the web version of this article.)

and Bangpakong rivers extends southwestward, forming a jet-like anticyclonic bulge near the river mouth and a downstream current along the coast with an average current speed of about 0.12 m/s. The salinity distribution shows a pattern of lower salinity in the north and higher in the south (~ 28). The distance of the bulge from the mouth of the Chaopraya River, as determined from the outmost isohaline that deflects toward the river mouth (label of 21.5 on the red line in Fig. 5b), is about 19.0 km offshore.

In November (Fig. 5c) when the northeasterly wind becomes stronger and the river discharge weakens, the freshwater inflow from the Charopraya and Bangpakong rivers flows directly to the southwest. Buoyant water from the Maeklong River stays close to the coast as it flows southward. During this period, the current is mainly a southwestward current (~ 0.16 m/s) likely associated with northeasterly monsoons.

In September and November, the river plume changes its extension direction with monsoons that are forced by the southwesterly wind and the northeasterly wind, respectively. Because the wind is relatively weak in October, a typical river plume can be found in the UGoT. Therefore, the primary controlling factor on the river plume in the UGoT is likely the wind.

In the bottom layer (Figs. 5d, e, f), salinity is higher than that in the

surface layer, and a similar spatial pattern is found with lower salinity in the north than in the south. The currents in the bottom layer are all northward currents, having the largest velocity in November (0.03 m/s).

The vertical profile of salinity along section AB (shown in Fig. 1b) shows stratification at the northern area of the UGoT that is stronger in October than in September and November (color, Figs. 5g, h, i). This is partly due to the low salinity water concentrating in the middle region of the UGoT in October relative to September, and partly due to the larger river discharge in October compared to November. Residual current along section AB (arrows, Figs. 5g, h, i) shows a structure of exchange current, with offshore flow in the surface layer and onshore flow in the bottom layer. The typical surface current speed is 0.03–0.10 m/s and the depth of no motion is at roughly 5 m. Both the surface current and bottom current are strongest in November, followed by October, and weakest in September.

In order to examine the stratification induced by the river discharge in the whole UGoT, we calculated the potential energy anomaly (PEA) in September and October (Fig. 6). This variable has been used in many studies as an indicator of vertical stratification (Simpson et al., 1977), and is calculated as follows.

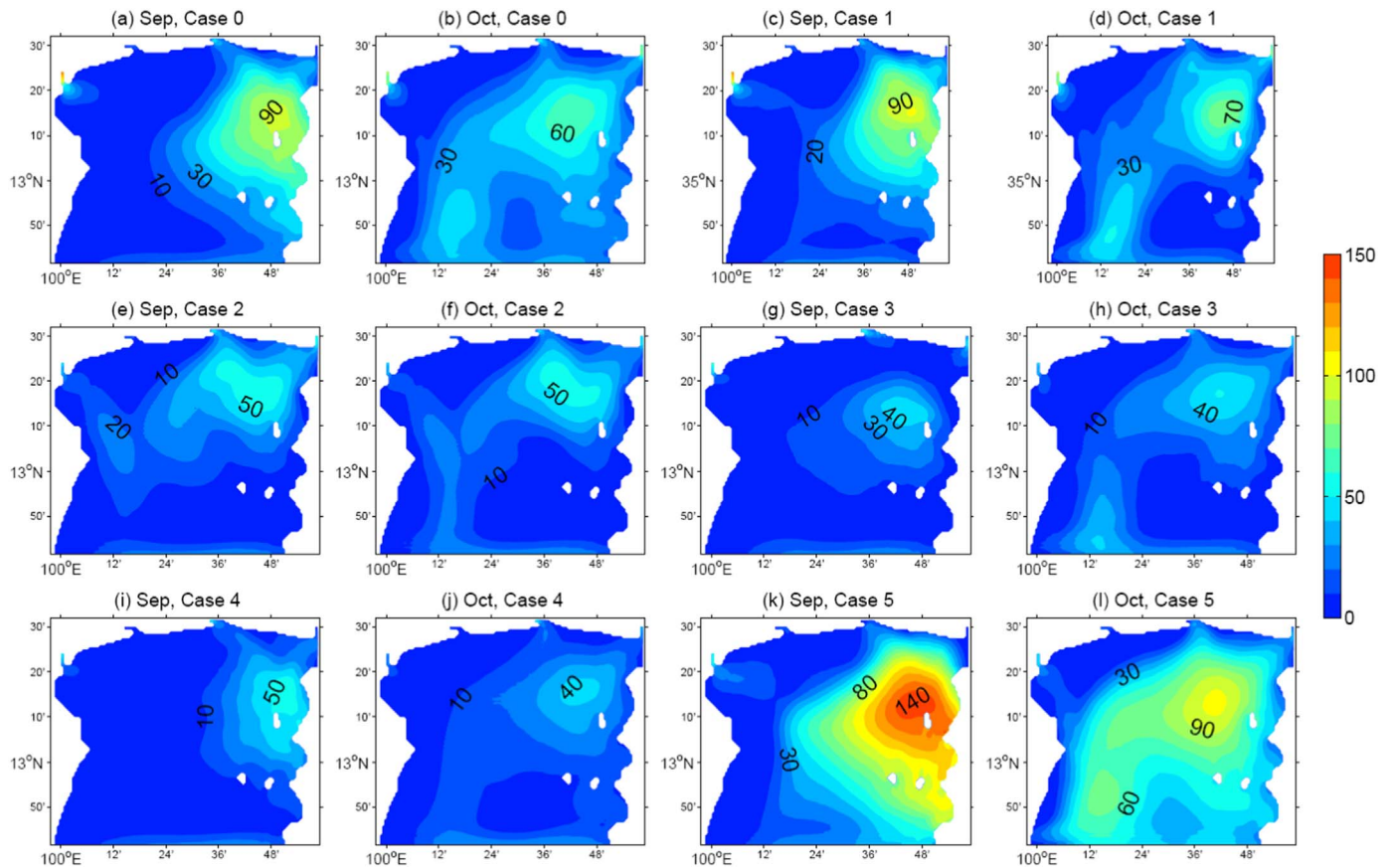


Fig. 6. Horizontal distribution of potential energy anomaly (J/m^3) in September and October for cases 0–5.

$$PEA = \frac{1}{h} \int_{-h}^0 (\rho - \bar{\rho})gzdz, \quad (1)$$

where h is the water depth, ρ is the water density, g is gravity acceleration, z is vertical coordinate with origin at sea surface and is positive upward, and $\bar{\rho} = \frac{1}{h} \int_{-h}^0 \rho dz$.

In September (Fig. 6a), the largest PEA ($> 90 J/m^3$) appears in the eastern part of the UGoT, while the smallest value appears in the west. In October (Fig. 6b), the largest PEA value ($\sim 65 J/m^3$) decreases but the area with a PEA greater than $30 J/m^3$ increases, covering almost the entire UGoT. The area with a large PEA is strongly stratified and hypoxia is easily generated in the bottom due to organic material decomposition.

4. Sensitivity study

In order to examine the effects of low latitude, wind and river discharge on the river plume in the UGoT, we conducted a series of numerical experiments (Table 2) in which we changed only one condition from the calculation shown in Section 3 (case 0) and ran the model with

Table 2
Model cases and external forcing factors.

Case 0	Case 1	Case 2	Case 3	Case 4	Case 5
12°N, tide, heating, river discharge, wind	35°N, tide, heating, river discharge, wind	12°N, tide, heating, river discharge, no wind	12°N, tide, heating, river discharge, wind (same Kz and Kv in case 2),	12°N, tide, heating, river discharge, 0.5 × river discharge, wind	12°N, tide, heating, 2 × river discharge, wind

all other conditions the same as in case 0. The modified condition was specified from start of model integration in these experiments. In case 1, we changed the latitude of the UGoT to about 35°N; in case 2, we set a wind stress of 0 over the entire UGoT; in case 3, we kept the same wind stress as in case 0 but switched off its influence on vertical mixing by using the vertical eddy viscosity coefficient and vertical eddy diffusivity coefficient from case 2; in cases 4 and 5, we multiplied the river discharges of the four rivers used in case 0 by a factor of 0.5 and 2.0, respectively.

4.1. Effects of latitude

4.1.1. Comparisons of salinity and residual current between middle and low latitudes

In September (Fig. 7a), since the prevailing southwesterly wind restrains the spread of the river plume, the effects of a change in latitude on the plume are very limited, with a slight difference in the vicinity of the Chaopraya and MaeKlong river mouths between case 1 and case 0. Low salinity water discharged from the Chaopraya River flows more southward in case 1 than in case 0, and that from the MaeKlong River flows more eastward in case 1 instead of northeastward as in case 0, which is a rightward deflection compared to that of case 0. In October (Fig. 7b) with the situation of a weak wind, the river plume around the Chaopraya River mouth in case 1 is markedly distinct compared to case 0. The anticyclonic bulge around the Chaopraya River mouth likely retreats to the coast, and is found at a smaller offshore distance of the bulge in case 1 (~ 16.0 km, shown by the red isohaline with a label of 19.5 in Fig. 7b) than in case 0 (~ 19.0 km). The reason we used different isohaline to define the bulge size in cases 0 and 1 is because the average salinity is different in two cases. Meanwhile, the downstream current flows more closely to the coast in case 1 than in case 0, which demonstrates that the coastal current is deflecting

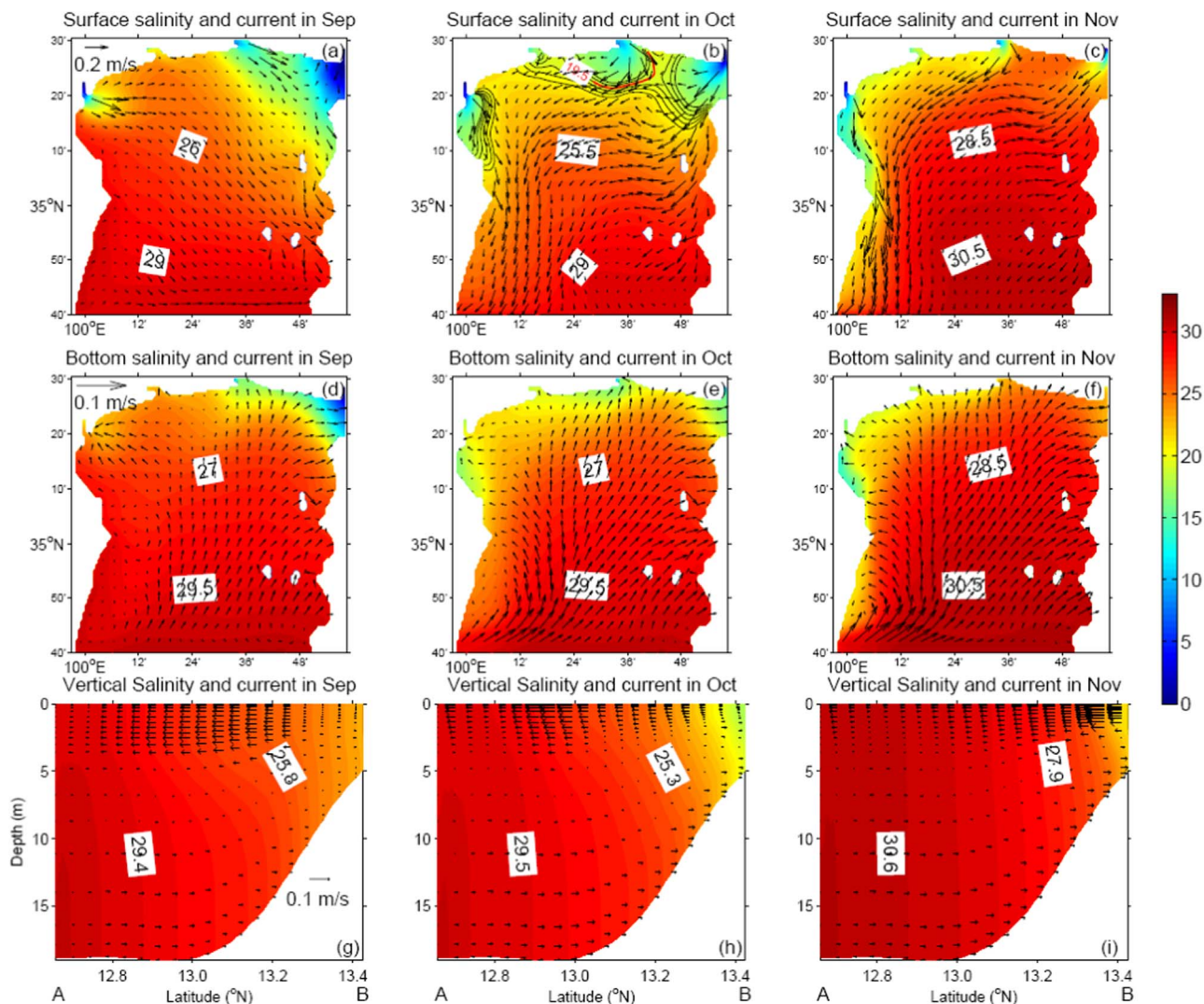


Fig. 7. The same as Fig. 5 but for case 1.

rightward with increasing latitude. The low salinity water from the Maeklong flows more southward along the west coast. The salinity in the northern area of the UGoT is lower in case 1 than in case 0. In November (Fig. 7c), when the wind blows from the northeast, the influence of the larger Coriolis force in case 1 than in case 0 is pronounced as low salinity water from the Chaopraya River flows westward more closely to the coast, resulting in a lower salinity in the northwest region of the UGoT compared to case 0. A similar result is also apparent at the Bangpakong River mouth, where the discharged water extends westward in case 1 instead of southwestward as in case 0. The low salinity water from the Maeklong also extends more southward along the west coast.

Saramul and Ezer (2014) reported that the larger Coriolis parameter in middle latitudes pushes the plume in the UGoT farther along the west coast and makes the plume less axisymmetric near the river mouth, but cannot turn the plume more to the right as compared to the low latitude case. The former two conclusions are also confirmed in our study. However, we found that the coastal current in the middle latitude case deflects more rightward along the coast, which will be explained in Section 4.1.2. Moreover, the bulge size around the Chaopraya River mouth in October is smaller in the middle latitude (16.0 km) than in the low latitude (19.0 km). The salinity in the northern area of the UGoT is lower in the middle latitude than in the low latitude, especially in October and November, which will also be discussed in Section 4.1.2.

The change in the bottom layer is mainly on the salinity value,

which is smaller in the northern area in case 1 (Figs. 7d, e, f) than in case 0. The residual current in the bottom layer shows little difference between the two cases.

The salinity along section AB shows a lower value in the northern UGoT (near point B) in case 1 than in case 0 (Figs. 7g, h, i). The southward component of the offshore current in the upper layer in October and November is weaker in the north in case 1 than in case 0, while there is little difference in the bottom onshore current between the two cases.

The PEA in case 1 shows a similar pattern to that in case 0, which has largest value in the east in September (Fig. 6c) and a large value in the entire UGoT in October (Fig. 6d). However, the PEA maximum is higher in case 1 than case 0.

Yankovsky and Chapman (1997) classified river plumes into three types: surface-advected plumes, bottom-advected plumes and intermediate plumes. Based on the vertical structure of the Chaopraya plume in October, we classify it as a surface-advected plume. The offshore distance of a surface-advected plume is calculated by $y_s = 2(3g'h_0 + v_i^2)/[(2g'h_0 + v_i^2)^{1/2}f]$ (Yankovsky and Chapman, 1997), where y_s is the offshore distance, g' is the reduced gravity based on the inflow density anomaly, $g' = g(\Delta\rho/\rho)$ (g is the gravity acceleration, ρ is the density of ambient water and $\Delta\rho$ is the density difference between the river plume and the ambient water at the river mouth), h_0 is the inflow depth, v_i is the inflow velocity, and f is the Coriolis parameter. The offshore distance of the bulge (y_s) has an inverse proportion

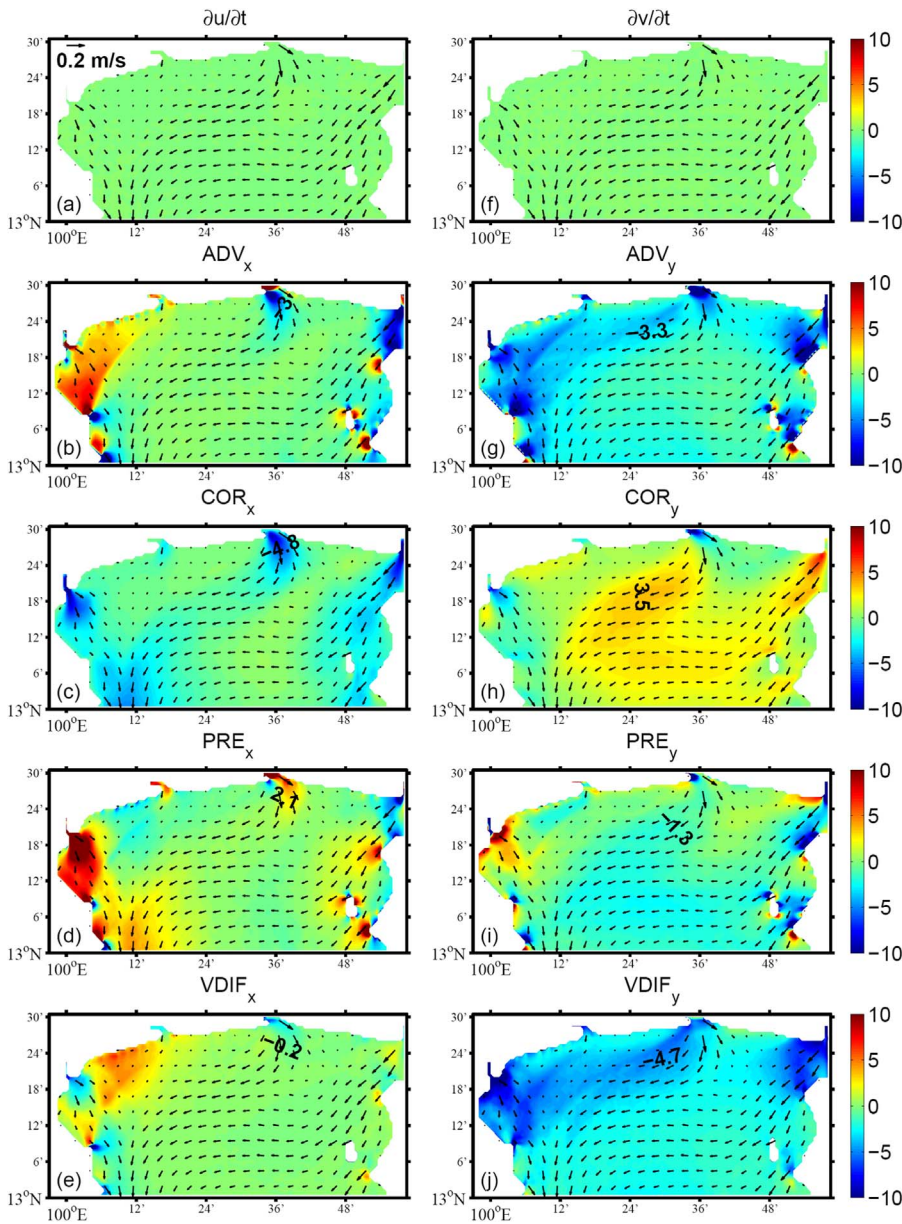


Fig. 8. Vertical averaged values of local acceleration, advection, Coriolis force, pressure gradient, and vertical viscosity (m/s^2 , color) in the momentum equation for eastward direction (left) and northward direction (right), and residual current (m/s , arrows) from the sea surface to the bottom of the offshore current in October for case 0. Values of momentum have been multiplied by a factor of 10^6 . (For interpretation of the references to color in this figure legend, the reader is referred to the web version of this article.)

relationship with the Coriolis parameter (f), which is $3.2 \times 10^{-5} \text{ s}^{-1}$ at 13°N and $8.3 \times 10^{-5} \text{ s}^{-1}$ at 35°N . The smaller Coriolis parameter in low latitudes favors a larger offshore distance. This is consistent with the result of a larger y_s in the low latitude (19 km, case 0) than in the middle latitude (16 km, case 1) in October when the wind is weak. However, the ratio of y_s between the low and middle latitudes is not exactly equal to that of $1/f$, indicating that the density difference between the river plume and the ambient water at the river mouth (g') also affects the offshore distance of the bulge because h_0 and v_i are the same in different latitudes.

4.1.2. Dynamics of the bulge and coastal current in middle and low latitudes

The momentum equation for the eastward and northward velocity of the plume can be expressed as

$$\frac{\partial u}{\partial t} + ADV_x = COR_x + PRE_x + VDIF_x \quad (2)$$

$$\frac{\partial v}{\partial t} + ADV_y = COR_y + PRE_y + VDIF_y \quad (3)$$

where ADV denotes the advection terms, COR denotes the Coriolis

force, PRE denotes the pressure gradient, and $VDIF$ denotes the internal stress divergence related to vertical eddy viscosity. The subscripts x and y denote the eastward and northward component, respectively. All terms are calculated by POM and the tidal components are removed with a tide killer filter (Hanawa and Mitsudera, 1985). The vertical averaged values of these terms from the sea surface to the bottom of the offshore current with low salinity are used to analyze the dynamics of the plume in different latitudes. The depth of the bottom of the offshore current with low salinity is determined from the vertical profiles of the northward component of the current. We mainly analyze the momentum of the bulge and coastal current in October, which are mid-field and far-field plumes, as described by Horner-Devine et al. (2015).

For the bulge in case 0 (low latitude), we mainly analyze the eastward momentum of the plume from the Chaopraya River. The acceleration term (Fig. 8a) is small, which means the velocity has little variation over time. The advection term (Fig. 8b) in the bulge is negative. The Coriolis force (Fig. 8c) is negative, which is associated with the southward current in the bulge. The pressure gradient (Fig. 8d) is positive. The term for internal stresses (Fig. 8e) is relatively small in the bulge. Therefore, the main balance is among the advection term,

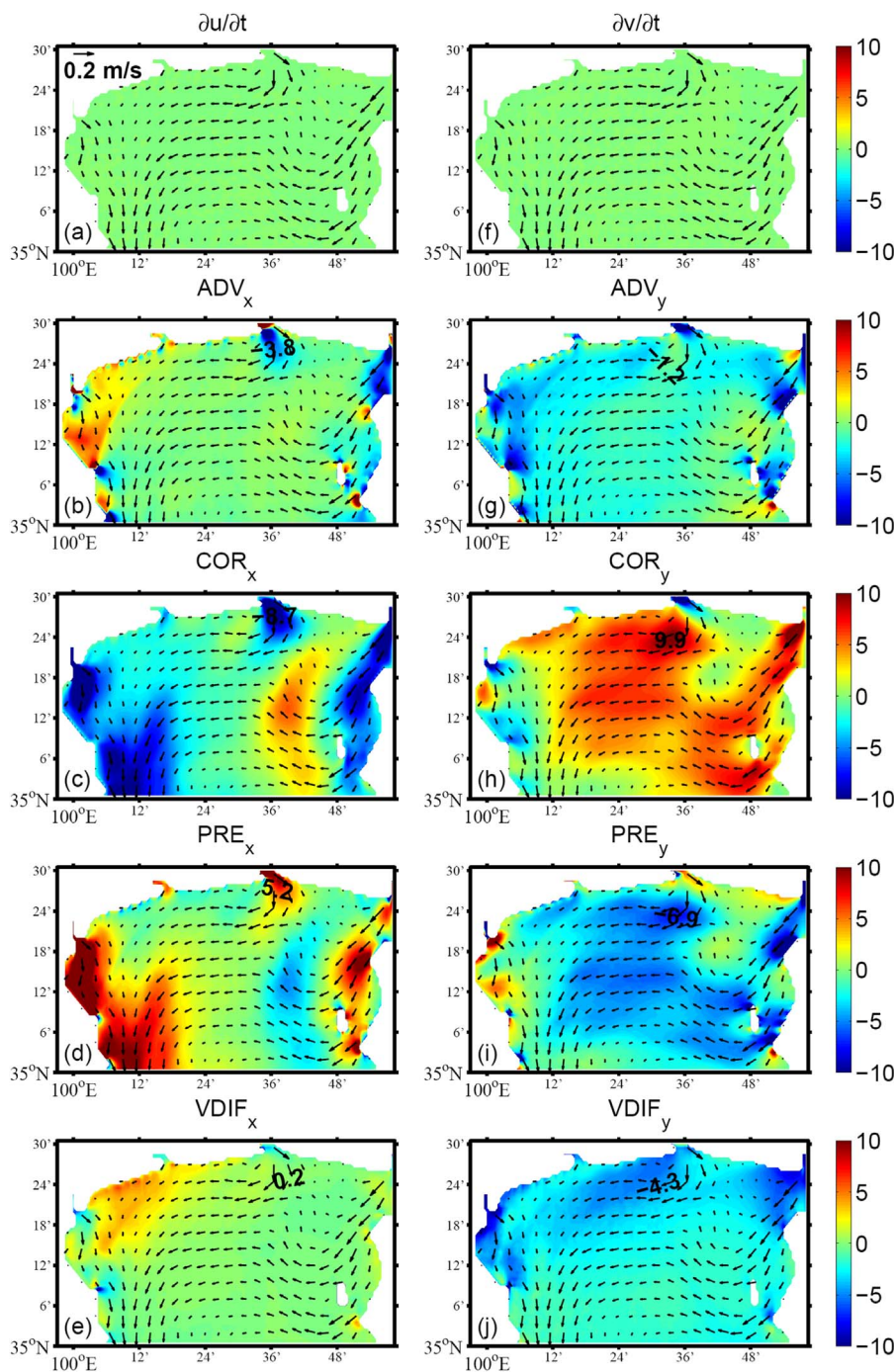


Fig. 9. The same as Fig. 8 but for case 1.

Coriolis force and pressure gradient for the bulge around the Chaopraya River mouth in a low latitude.

Moving to the middle latitude (case 1), the eastward momentum balance for the bulge around the Chaopraya River mouth is still driven by advection, the Coriolis force and the pressure gradient (Figs. 9b, c, d). However, both the Coriolis force (Fig. 9c) and pressure gradient (Fig. 9d) are increased compared to case 0. Since the Coriolis parameter is $3.2 \times 10^{-5} \text{ s}^{-1}$ at 13°N and $8.3 \times 10^{-5} \text{ s}^{-1}$ at 35°N , and the current speed does not change greatly, the Coriolis force increases more than two-fold in case 1 compared to case 0. The reason for the increase in pressure gradient will be explained later.

For the coastal current, we mainly analyze the northward momentum of the Chaopraya River plume. In case 0, the acceleration term (Fig. 8f) is smaller than the other terms by one order. The advection

term (Fig. 8g) is negative in the coastal current. The Coriolis force (Fig. 8h) is positive, while the pressure gradient (Fig. 8i) and internal stresses (Fig. 8j) are both negative. The momentum balance of the coastal current in case 0 is likely maintained by the advection term, Coriolis force, pressure gradient and internal stresses. The ratio for the advection term, Coriolis force, pressure gradient and internal stresses is approximately 2:2:1:3.

Moving to the middle latitude (case 1), the Coriolis force (Fig. 9h) and pressure gradient (Fig. 9i) increase greatly, while the advection term (Fig. 9g) and internal stresses (Fig. 9j) remain almost the same as in case 0. The larger Coriolis force near the coast demonstrates the importance of the Coriolis force in middle latitudes, which tends to make the buoyant water turn more rightward along the coast. The ratio of the advection term, Coriolis force, pressure gradient and internal

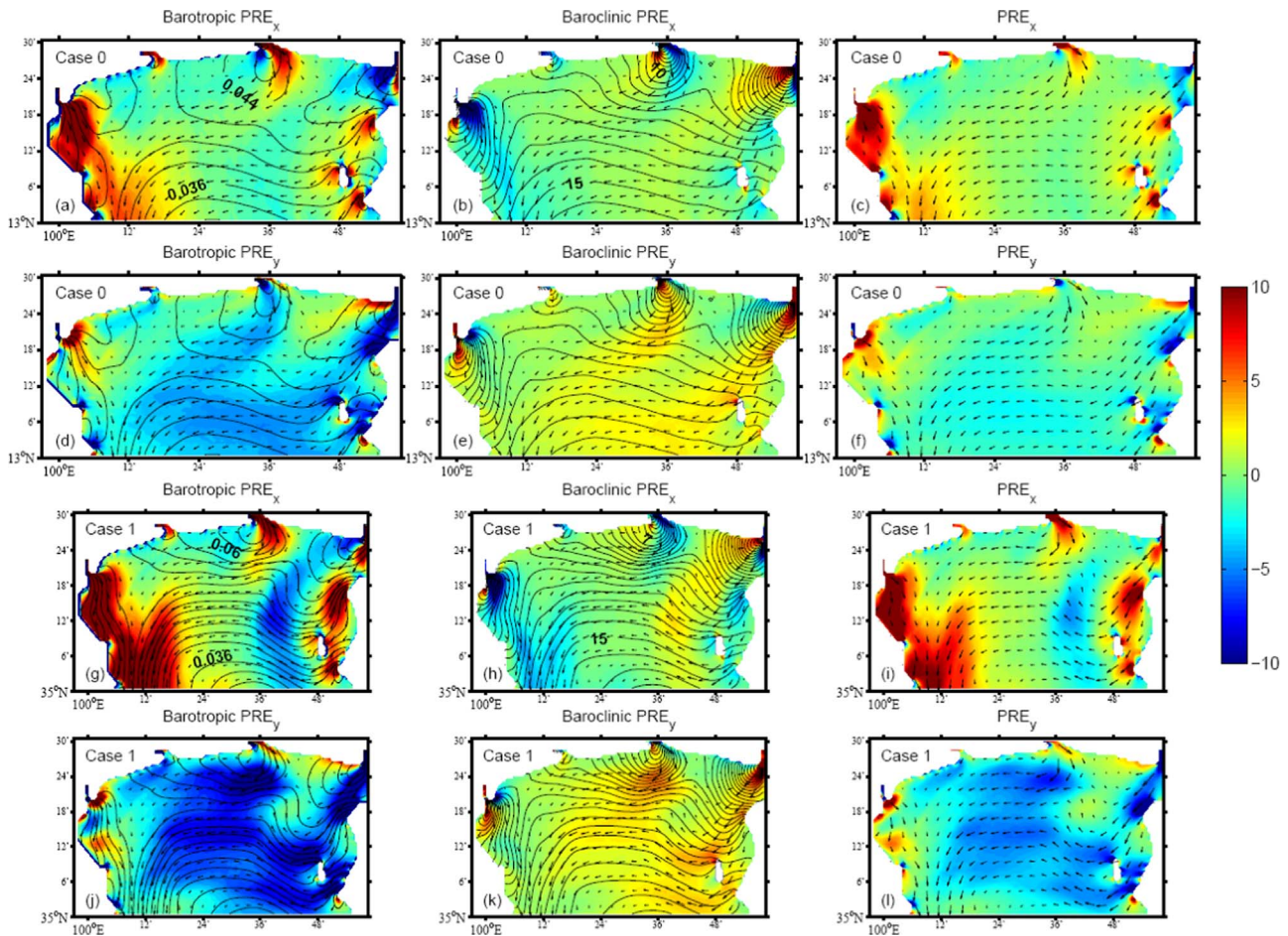


Fig. 10. Vertical averaged values (m/s^2) of barotropic pressure gradient (left), baroclinic pressure gradient (middle), and their sum (right) for the eastward direction (x-direction) and northward direction (y-direction) from the sea surface to the bottom of the offshore current in October. The black lines in the left panels indicate the elevation in the surface layer, while those in middle panels show the vertical averaged density. The upper six panels are for case 0, while the lower six panels are for case 1. The arrows show the vertical averaged residual current. Values of momentum have been multiplied by a factor of 10^6 . The smaller zonal range for case 1 is caused by its relatively higher latitude location than case 0.

stresses is approximately 1:6:4:3 in the middle latitude, indicating that the coastal current in the middle latitude becomes more geostrophic relative to that in the low latitude.

To explain the variation in the pressure gradient in case 0 and case 1, we decomposed the pressure gradient into the barotropic component induced by the horizontal gradient of water level and the baroclinic component induced by the horizontal gradient of density. In case 0, the eastward barotropic component of the pressure gradient (color, Fig. 10a) in the bulge around the Chaopraya River mouth has opposite signs: positive in the east and negative in the west. This is because the elevation (lines, Fig. 10a) is higher in the central than in the east and west as freshwater runs out from the river mouth. The baroclinic component of the pressure gradient (color, Fig. 10b) is opposite to the barotropic component of the pressure gradient, which is negative in the east and positive in the west of the bulge around the Chaopraya River mouth. The density (lines, Fig. 10b) in the central is smaller than that in the west and east. The sum of the barotropic and baroclinic components shows a positive pressure gradient in the bulge of the Chaopraya (Fig. 10c). For the coastal current from the Chaopraya River, the northward barotropic component of pressure gradient (color, Fig. 10d) is negative, which is induced by the higher elevation in the north than in the south (lines, Fig. 10d). On the other hand, the baroclinic component of the pressure gradient (color, Fig. 10e) is positive due to the larger density in the south than in the north (lines, Fig. 10e). The larger barotropic component relative to baroclinic component produces a negative pressure gradient in the coastal current (Fig. 10f).

Moving to the middle latitude (case 1), the eastward barotropic

component of the pressure gradient in the bulge (color, Fig. 10g) and the northward barotropic component of the pressure gradient in the coastal current (color, Fig. 10j) from the Chaopraya River increase. It is likely that more freshwater flows out from the bulge, and induces the closer elevation contour (lines, Fig. 10g) relative to case 0 (lines, Fig. 10a). The northward baroclinic component of the pressure gradient (color, Fig. 10k) also increases due to more freshwater flowing out from the bulge, which enlarges the density gradient (lines, Fig. 10k) in case 1. The greater increase in the barotropic component relative to the baroclinic component in case 1 results in a larger pressure gradient in case 1 (Figs. 10i, l) than in case 0 (Figs. 10c, f).

According to Fong and Geyer (2002), the shape of the bulge and the freshwater carried out by the coastal current are dependent on the Rossby number. For a large Rossby number, the shape of the bulge is circular, and the transport of the coastal current is smaller; for a small Rossby number, the shape of the bulge is semi-circular, and the transport of the coastal current is larger. Fong and Geyer (2002) explain this occurrence using the Nofs (1988) theory on baroclinic eddies colliding with a wall, in which a nonlinear, layered, analytic model is used to determine how an eddy interacts with a wall. When a quasi-geostrophic anticyclonic eddy interacts with a wall, it will leak fluid toward the right-hand side (looking offshore in the northern hemisphere). If only the outer edge of the eddy interacts with a wall, the leakage from the eddy is small; if the eddy is closer to the wall, the leakage is larger.

The eddy and the leakage are analogous to the bulge and the freshwater carried out by the coastal current. In low latitudes with a small Coriolis parameter (f), the Rossby number is large, which leads to

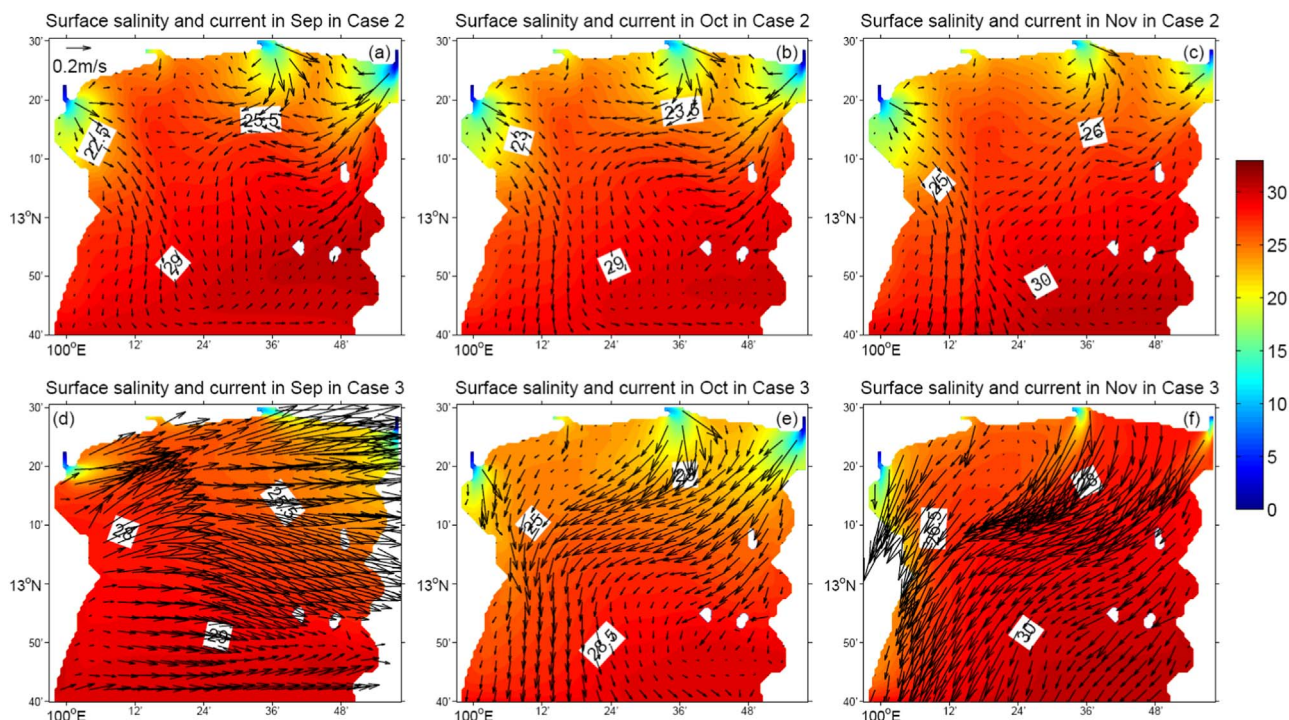


Fig. 11. Horizontal distribution of surface salinity (color) and residual current (m/s, arrows) in September, October, and November for case 2 (top) and case 3 (bottom). (For interpretation of the references to color in this figure legend, the reader is referred to the web version of this article.)

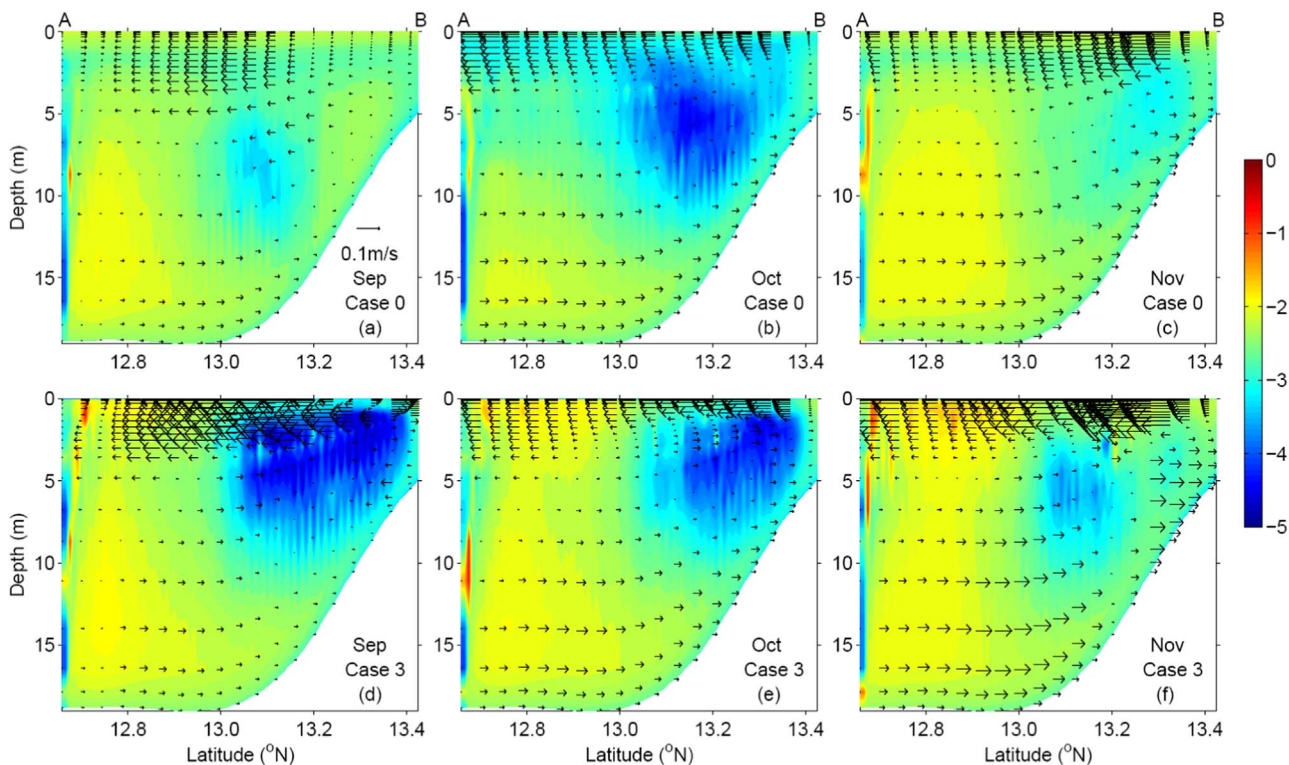


Fig. 12. Vertical distribution of vertical eddy viscosity $\text{Log}_{10}(K_z)$ (m^2/s , color) and current along section AB (m/s, arrows) in September, October and November for case 0 (top) and case 3 (bottom).

a large offshore distance of the bulge (eddy away from the wall), and consequently the freshwater quantity flowing with the coastal current is smaller. In middle latitudes, the situation is opposite; that is, the bulge is smaller (eddy close to the wall) and the freshwater quantity flowing with the coastal current is larger. This can explain why the barotropic and baroclinic pressure gradient is larger in the middle latitude than in

the low latitude, as well as the lower salinity in the northern UGoT in case 1 than in case 0.

4.2. Effects of wind

The effect of wind on the coastal region is manifested not only in the

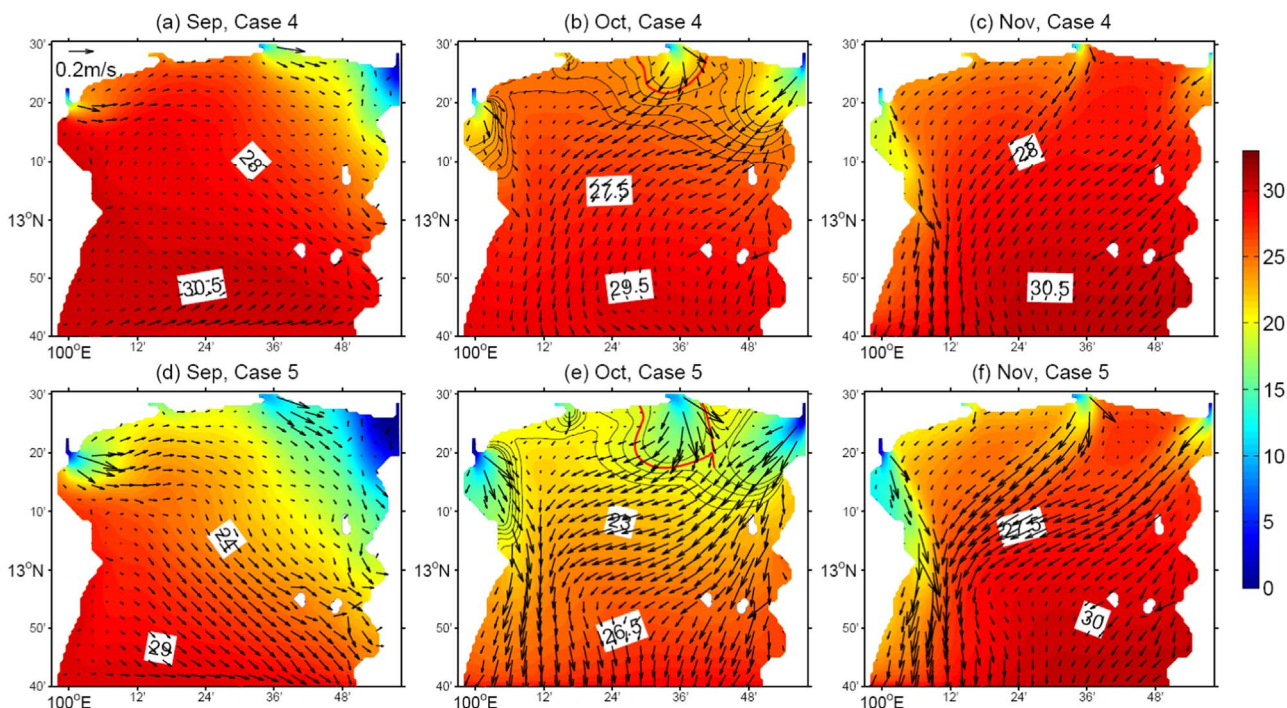


Fig. 13. Horizontal distribution of surface salinity (color) and residual current (m/s, arrows) in September, October and November for case 4 (top) and case 5 (bottom). The black lines in (b) and (e) show the isohalines around the bulge, and the red lines indicate the position of the offshore distance of the bulge. (For interpretation of the references to color in this figure legend, the reader is referred to the web version of this article.)

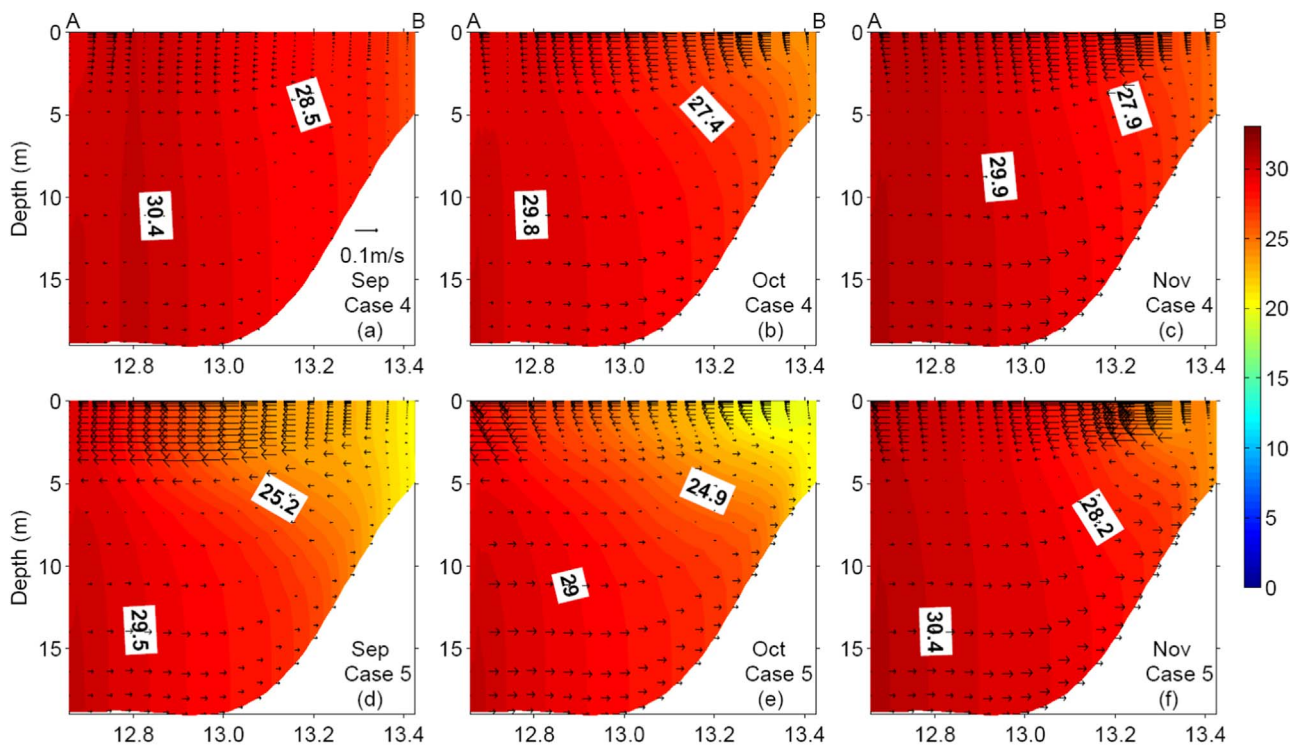


Fig. 14. Vertical distribution of salinity (color) and current (m/s, arrows) along section AB in September, October and November for case 4 (top) and case 5 (bottom). (For interpretation of the references to color in this figure legend, the reader is referred to the web version of this article.)

changing surface current but also in producing enhanced vertical mixing in the upper layer. To separately examine the two effects of wind on the river plume, we consider the situation of no wind in case 2 and the situation of wind but without wind-enhanced vertical mixing in case 3 by using the vertical eddy viscosity and diffusivity from case 2.

In case 2, when there is no wind, the structures of the river plume in

different months are almost identical, with a bulge forming near the river mouth, and a downstream current flowing along the coast (Figs. 11a, b, c). The only difference among the months is the salinity value and current speed, which are determined by monthly river discharges. The coastal current speed from the Chaopraya River is 0.18, 0.15, and 0.11 m/s in September, October, and November, respectively.

The PEA shows a similar pattern in September and October (Figs. 6e, f), with a large value around the Chaopraya and Bangpakong rivers, and a higher value in September due to larger river discharge.

In case 3, the surface currents (Figs. 11d, e, f) are different from those in case 2, but show a resemblance to those in case 0 in current direction with a larger current speed than case 0. Comparison of case 3 and case 2 shows a wind-induced surface current in case 3 that flows northeastward in September and southwestward in October and November under the southwesterly and northeasterly winds, respectively. The coastal current speed from the Chaopraya River in case 3 is 0.36, 0.22, and 0.40 m/s in September, October, and November, respectively. Comparison of case 3 with case 0 shows the effect of wind in strengthening the vertical mixing, which weakens the current speed in case 0, especially in the northern area of 13°N. The distribution of PEA in case 3 shows a similar pattern to that in case 0, which is large in the east in September and large in the entire UGoT in October (Figs. 6g, h).

Wind produces large vertical eddy viscosity in case 0 (color, Figs. 12a, b, c) relative to cases 2 and 3 (color, Figs. 12d, e, f) in the upper layer north of 13°N. Large eddy viscosity results in strong internal friction and therefore weakens the current speed in the surface layer in case 0 (arrows, Fig. 12). Weaker offshore current in the surface layer induces a weaker onshore current in the bottom layer in case 0 (arrows, Fig. 12).

4.3. Effects of river discharge

We examined the influence of river discharge on the river plume by cutting it in half and doubling in cases 4 and 5, respectively. In case 4 (case 5), expansions of the river plume (Fig. 13) are similar to those in case 0, but with higher (lower) salinity and weaker (stronger) downstream current than in case 0. The offshore distance of the bulge from the Chaopraya River in October increases from 15.7 km in case 4 to 23.5 km in case 5 (red lines, Figs. 13b, e). The coastal current from the Chaopraya River in October also turns more rightward (looking offshore) with increasing river discharge. The response of the plume to the magnitude of the river discharge in the UGoT is similar to that in the Yellow River (Wang et al., 2008) in both plume range and orientation.

The vertical profiles of salinity show the strongest stratification in case 5 (color, Figs. 14d, e, f), followed by case 0 (color, Figs. 5g, h, i) and case 4 (color, Figs. 14a, b, c) in the northern part of the UGoT. The larger river discharge and stronger stratification enhance the surface offshore current and bottom onshore current in case 5 (arrows, Figs. 14d, e, f).

The patterns of PEA in cases 4 and 5 are similar to those in case 0, but with a smaller maximum value in case 4 (Figs. 6i, j) and a larger one in case 5 (Figs. 6k, l). The largest PEA in case 4 is 50 J/m³ in September and 40 J/m³ in October, while it is 140 J/m³ and 95 J/m³ in case 5. Therefore, the river discharge can significantly change stratification in the UGoT in the rainy season, and influence the situation of hypoxia there.

5. Conclusion

Differing from the Amazon River plume that extends leftward to the northern hemisphere, in the UGoT, the river plume from four rivers in the head of the gulf is significantly influenced by monsoons. The river plume extends northeastward under southwesterly winds during the period from May to September and southwestward under northeasterly winds during the period from November to January. In October, a transitional period for monsoons with lower wind speeds, a typical river plume with an anticyclonic bulge near the river mouth and a downstream current along the coast can be found in the UGoT. Stratification induced by river discharge is also influenced by monsoons, and is strong in the eastern part of the gulf in September but expands over the entire gulf in October, which has importance on the generation of hypoxia in the UGoT.

Changing the model domain to the middle latitude results in a different river plume in the UGoT. The bulge near the river mouth extends farther offshore in the low latitude than in the middle latitude, which can be qualitatively explained by the inverse relationship between the offshore distance of bulge and the Coriolis parameter in a surface-advected plume (Yankovsky and Chapman, 1997). Geostrophic control on the coastal current of the plume is weaker in the low latitude than in the middle latitude, which induces a smaller rightward deflected angle of the coastal current in the low latitude than in the middle latitude. Furthermore, salinity in the model domain is higher in the low latitude than in the middle latitude. This is associated with less freshwater being carried out by the coastal current from the bulge in the low latitude than in the middle latitude, which is consistent with the theory of Nof (1988). All these points were either not reported by or are different from the previous study on the river plume in the UGoT (Saramul and Ezer, 2014).

Wind has two effects on the surface current that acts as the ambient current of the river plume: directly changing the surface current with the addition of momentum to the water and indirectly changing the surface current with enhancement of vertical mixing. These effects have not been reported in previous studies. River discharge can change the size of the bulge and the strength of the coastal current of the river plume. It also significantly influences stratification in the UGoT. A larger river discharge tends to induce stronger stratification.

Acknowledgements

This study was supported by JSPS KAKENHI Grant Number 26302001 and by grants from the government to national university corporations for the Joint Usage/Research Center, MEXT, Japan and JSPS Core-to-Core Program.

References

- Blumberg, A.F., Mellor, G.L., 1987. A description of a three dimensional coastal ocean circulation model. In: Heaps, N. (Ed.), *Three-Dimensional Coastal Ocean Models*, Coastal Estuarine Stud. 4. AGU, Washington, D.C., pp. 1–16 (208pp).
- Buranapratheprat, A., Yanagi, T., Matsumura, S., 2008. Seasonal variation in water column conditions in the upper Gulf of Thailand. *Cont. Shelf Res.* 28, 2509–2522.
- Buranapratheprat, A., Niemann, K.O., Yanagi, T., Matsumura, S., Sojisuporn, P., 2009. Circulation in the upper Gulf of Thailand investigated using a three-dimensional hydrodynamic model. *Burapha Sci. J.* 14 (1), 99–113.
- Chao, S.-Y., Boicourt, W.C., 1986. Onset of estuarine plumes. *J. Phys. Oceanogr.* 16, 2137–2149.
- Dzwonkowski, B., Park, K., Lee, J., Webb, B.M., Valle-Levinson, A., 2014. Spatial variability of flow over a river-influenced inner shelf in coastal Alabama during spring. *Cont. Shelf Res.* 74, 25–34.
- Fong, D.A., 1998. *Dynamics of Freshwater Plumes: Observations and Numerical Modelling of the Wind-forced Response and Alongshore Freshwater Transport* (Ph.D. Dissertation). MIT-Woods Hole Oceanographic Institution.
- Fong, D.A., Geyer, W.R., 2002. The alongshore transport of freshwater in a surface-trapped river plume. *J. Phys. Oceanogr.* 32, 957–972.
- Green, R.E., Bianchi, T.S., Dagg, M.J., Walker, N.D., Breed, G.A., 2006. An organic carbon budget for the Mississippi River turbidity plume and plume contributions to air–sea CO₂ fluxes and bottom water hypoxia. *Estuaries Coasts* 29, 579–597.
- Guo, X., Valle-Levinson, A., 2007. Tidal effects on estuarine circulation and outflow plume in the Chesapeake Bay. *Cont. Shelf Res.* 27, 20–42.
- Hanawa, K., Mitsudera, H., 1985. On daily average of oceanographic data (in Japanese). *Coast. Oceanogr. Bulletin* 23, 79–87.
- Horner-Devine, A., Jay, D., Orton, P., Spahn, E., 2009. A conceptual model of the strongly tidal Columbia River plume. *J. Mar. Syst.* 78, 460–475.
- Horner-Devine, A., Hetland, R., MacDonald, D., 2015. Mixing and transport in coastal river plumes. *Annu. Rev. Fluid Mech.* 47, 569–594.
- Kasai, A., Hill, A.E., Fujiwara, T., Simpson, J.H., 2000. Effect of the Earth's rotation on the circulation in regions of freshwater influence. *J. Geophys. Res.* 105 (C7), 16961–16969.
- Lentz, S.J., 1995a. Seasonal variations in the horizontal structure of the Amazon Plume inferred from historical hydrographic data. *J. Geophys. Res.* 100, 2391–2400.
- Lentz, S.J., 1995b. The Amazon River Plume during AMASSEDs: subtidal current variability and the importance of wind forcing. *J. Geophys. Res.* 100, 2377–2390.
- Lentz, S.J., Limeburner, R., 1995. The Amazon River plume during AMASSEDs: spatial characteristics and salinity variability. *J. Geophys. Res.* 100 (C2), 2355–2375.
- Mellor, G.L., 2003. *Users guide for a three-dimensional, primitive equation, numerical ocean model (2003 version)* (report, 53 pp.). Program in Atmosphere and Ocean Science. Princeton Univ., Princeton, N. J.

- Mellor, G.L., Yamada, T., 1982. Development of a turbulence closure model for geophysical fluid problems. *Rev. Geophys.* 20, 851–875.
- Münchow, A., Garvine, R.W., 1993. Dynamical properties of a buoyancy-driven coastal current. *J. Geophys. Res.* 98 (C11), 20063–20077.
- Nittrouer, C.A., DeMaster, D.J., 1996. The Amazon shelf setting: tropical, energetic, and influenced by a large river. *Cont. Shelf Res.* 16, 553–573.
- Nof, D., 1988. Eddy-wall interactions. *J. Mar. Res.* 46, 527–555.
- Pritchard, D.W., 1952. Salinity distribution and circulation in the Chesapeake Bay estuarine system. *J. Mar. Res.* 11, 106–123.
- Pritchard, D.W., 1954. A study on the salt balance in a coastal plain estuary. *J. Mar. Res.* 13, 133–144.
- Saramul, S., Ezer, T., 2014. On the dynamics of low latitude, wide and shallow coastal system: numerical simulations of the Upper Gulf of Thailand. *Ocean Dyn.* 64, 557–571.
- Simpson, J.H., Hughes, D.G., Morris, N.C.G., 1977. The relation of seasonal stratification to tidal mixing on the continental shelf. *Deep Sea Res.* 24 (Suppl), 327–340.
- Smagorinsky, J.S., 1963. General circulation experiments with the primitive equations. I. The basic experiment. *Mon. Weather Rev.* 91, 99–164.
- Thadathil, P., Gopalakrishna, V.V., Muraleedharan, P.M., Reddy, G.V., Araligidad, N., Shenoy, S., 2002. Surface layer temperature inversion in the Bay of Bengal. *Deep Sea Res. Part I* 49, 1801–1818.
- Wang, Q., Guo, X., Takeoka, H., 2008. Seasonal variations of the Yellow River plume in the Bohai Sea: a model study. *J. Geophys. Res.* 113, C08046.
- Wang, Y., Liu, Z., Gao, H., Ju, L., Guo, X., 2011. Response of salinity distribution around the Yellow River mouth to abrupt changes in river discharge. *Cont. Shelf Res.* 31, 685–694.
- Wong, K.-C., 1994. On the nature of transverse variability in a coastal plain estuary. *J. Geophys. Res.* 99, 14209–14222.
- Yankovsky, A.E., Chapman, D.C., 1997. A simple theory for the fate of buoyant coastal discharges. *J. Phys. Oceanogr.* 27, 1386–1401.
- Yankovsky, A.E., Hickey, B.M., Münchow, A.K., 2001. Impact of variable inflow on the dynamics of a coastal plume. *J. Geophys. Res.* 106, 19809–19824.